JTTEE5 15:431-437
DOI: 10.1361/105996306X124446
1059-9630/$19.00 © ASM International

Corrosion Behavior of Wire-Arc-Sprayed Stainless Steel Coating on Mild Steel

Z. Zeng, N. Sakoda, and T. Tajiri

(Submitted August 4, 2005; in revised form November 14, 2005)

The corrosion characteristics of a wire-arc-sprayed stainless steel coating on mild steel have been investigated in regards to atomizing gases and sealing treatment. Salt spray test was performed. The corrosion behavior of the coating was observed under a microscope successively through a cycling test of wetting and drying in a salt solution. The sealing-treated coating was found to rust faster compared with the non-sealing-treated coating; it protected the mild steel substrate against corrosion, but even it deteriorated the coating itself due to the interruption of the substrate as an anode. The air-atomized coating rusted more heavily than the nitrogen-atomized one. Four different phases were observed in the coating in regards to corrosion behavior; namely, chromium-based oxide, iron-based oxide, chromium-depleted metallic phase, and stainless steel matrix phase. It was found that the chromium-depleted metallic phase and the iron-based oxide are non-corrosion-resistant, whereas the chromium-based oxide and the stainless steel matrix phase are corrosion-resistant.

Keywords corrosion, salt spray test, stainless steel coating, wire arc spraying

1. Introduction

Wire-arc-sprayed coatings of austenite stainless steel have been widely applied to component parts of various machines and equipment owing to their low cost, good performance, and field applicability. Compressed air is generally used to atomize molten droplets to form a coating due to its availability and economy. However, air-atomized stainless steel coatings include large amounts of oxides and pores, which have detrimental effects on coating properties. Oxides in a coating may not only decrease the cohesion strength between particles and the adhesion strength between the coating and substrate, but also degrade the corrosion resistance of the coating due to the formation of local electrochemical cells in the coating. Pores, particularly open pores, allow corrosive gases or fluids to permeate to the substrate and reduce the ability of the coating to prevent corrosion.

To improve wire-arc-sprayed coatings, their oxide content and number of pores should be minimized. Many efforts have been made up to the present for this purpose. For example, the use of inert gases as atomizing gas, attaching a mechanical shroud to a spray gun and designing new arc spray gun units have been developed to form high-integrity coatings. However, it is still desired to form better coatings without losing their competitive cost and to increase the endurance and reliability of stainless steel coatings in terms of service life.

There are some reports on the effectiveness of using an inert atomizing gas and sealing treatment to extend the service life of stainless steel coatings. For example, the corrosion resistance of 316L stainless steel coatings sprayed by the wire-arc process using nitrogen and argon gases is superior to that of conventional air-arc-sprayed stainless steel coatings. However, the coatings sprayed with inert gases still suffer localized corrosion associated with small pores and crevice corrosion (Ref 1). Organic or inorganic sealant materials are usually applied to the coatings to fill pores. Such sealing treatment improves the corrosion resistance of air-arc-sprayed coatings (Ref 2). However, in some cases, sealing treatment could deteriorate the coatings thereby accelerating corrosion (Ref 3).

In this study, the aim is to investigate the corrosion behavior of coating in detail to understand the effect of an inert atomizing gas and sealing treatment on such behavior.

2. Experimental Procedure

A commercial base austenite stainless steel wire, Japanese Industrial Standard (JIS)-316L (Ref 4), containing 17.0% chromium, 13.5% nickel, and 2.5% molybdenum in mass% was arc-sprayed using a twin-wire-arc spray unit of TAFA8830. Arc spraying was performed on a mild steel substrate under the conventional conditions as follows: arc voltage, 30V; arc current, 300A; spray distance, 150 mm; atomizing pressure, 380 kPa; and airflow, 2.1×10^{-2} m^3/s. Two different gases, air and nitrogen, were used as atomizing gases. The thickness of the coating was about 500 μm. The coatings were ground to 350 μm in thickness to make the thickness of the coatings uniform. Some of the specimens were treated with an air drying phenolic sealer (Metcoseal

Zhensu Zeng, Nobuaki Sakoda, and **Toshiro Tajiri,** Kurashiki Boring Kiko Co., Research and Development, 329-2 Ebana, Jitoukami, Kamogata-cho, Asakuchi-gun, Okayama 719-0233 Japan. Contact e-mail: zeng@kbknet.co.jp.

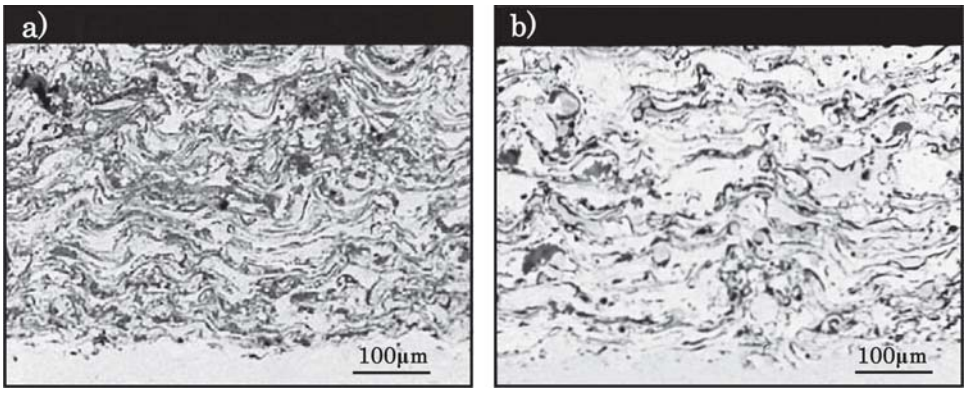

Fig. 1 Microstructures of coatings; (a) air-atomized and (b) nitrogen-atomized

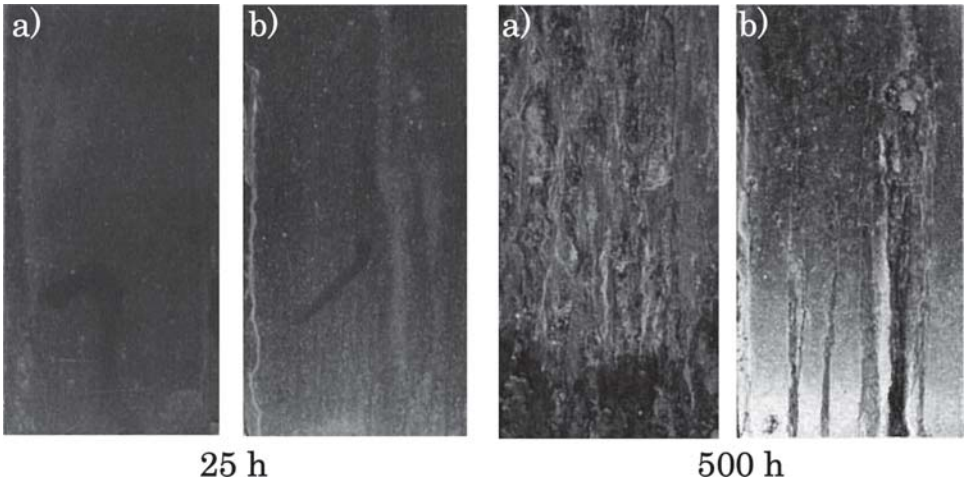

Fig. 2 Surface appearances of coatings with non-sealing treatment after salt spray tests of 25 and 500 h; (a) air-atomized and (b) nitrogen-atomized

AP, Sulzer Metco Ltd., Tokyo, Japan) to examine the effect of sealing treatment on the corrosion behavior. Salt spray tests were performed to investigate the corrosion property of the specimens up to 500 h in accordance with the standard JIS-Z-2371 (Ref 5). The temperatures of the 5 mass% salt solution and the chamber were maintained at 320 ± 1 and 308 ± 1 K, respectively.

The local electric distribution was measured on the surfaces of thermal sprayed coatings by using a Kelvin force microscopy (KFM) (Ref 6, 7). Scanning probe microscope (SPM) (SPI3800N, Seiko Instrument Inc., Chiba, Japan) equipped with KFM mode was applied to measure the topography and the electrical potential distribution of the surface simultaneously under the normal ambient conditions. The observed area is 30 × 30 μm on cross section of the coating, which was polished with 1 μm diamond paste. The same area of the KFM image was also observed by a use of scanning electron microscope (SEM) (S-3000H, Hitachi Science Systems, Ltd., Ibaraki, Japan) and energy dispersive x-ray (EDX) analysis was carried out.

To examine the corrosion behavior of different phases in the coatings more precisely, a polished surface was observed successively under a microscope through repeated cycling tests of dipping for 1 h in 5 mass% salt solution and drying for 1 h under atmospheric condition.

3. Results and Discussion

3.1 Microstructure and Salt-Spray Test

Microstructures in the cross section of the coatings sprayed by air atomization and nitrogen atomization are shown in Fig. 1(a) and (b). White areas correspond to the metallic phase, gray areas are the oxide phases, and black spots are pores. It is seen that both coatings have high oxide content and a number of pores. The amounts of oxides and pores in the microstructures were measured to be about 48 and 36% in area for the air atomization and nitrogen atomization, respectively, using image analysis.

Figure 2(a) and (b) shows the surface appearances of the air-atomized and nitrogen-atomized specimens, which were not subjected to sealing treatment, after 25 and 500 h of salt spray test, respectively. Little rust is visible on both coatings after 25 h of salt spray testing. The coatings rust remarkably after 500 h and the air-atomized coating seems to rust more significantly than the nitrogen-atomized coating. It is suggested from this result that the air-atomized coating may be less dense than the nitrogen-atomized coating. On the other hand, the surfaces of the specimens treated with a phenolic sealer rust at 25 h regardless

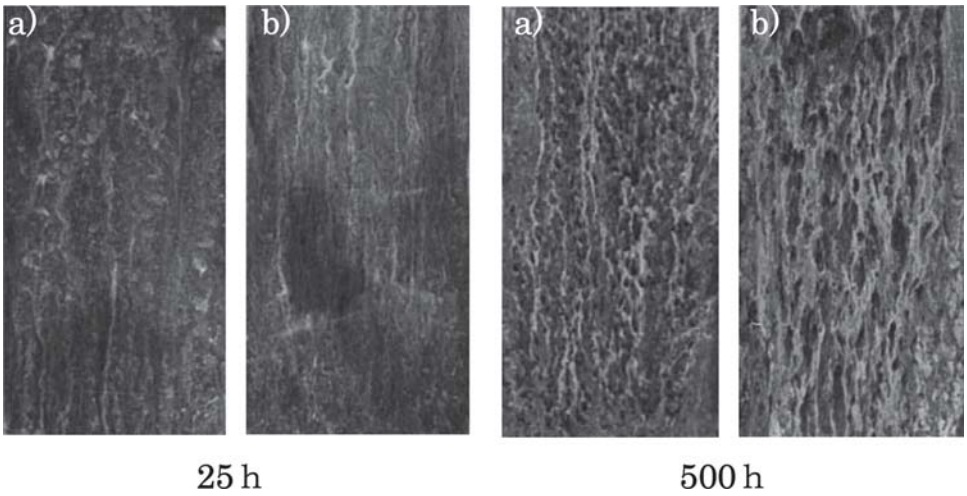

Fig. 3 Surface appearances of coatings with sealing treatment after salt spray tests of 25 and 500 h; (a) air-atomized and (b) nitrogen-atomized

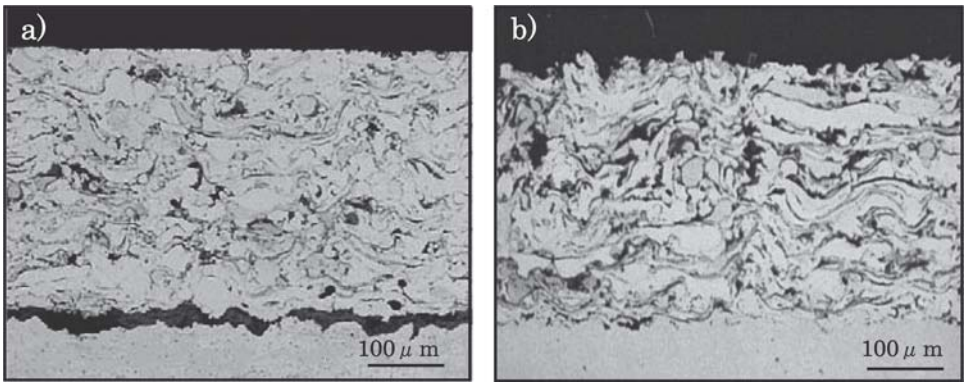

Fig. 4 Microstructures of nitrogen-atomized coating after salt spray testing; (a) unsealed coating and (b) sealed coating

of the difference in the type of atomizing gas used, as shown in Fig. 3. It is noted that the sealing-treated specimens rust more markedly than the non-treated ones.

Figure 4 shows microstructures on the cross section of nitrogen-atomized coatings with and without sealing treatment after 500 h of salt spray test. The corrosion behavior obviously differs between the non-sealing-treated and sealing-treated specimens. The interface of the mild steel substrate is preferentially corroded in the non-sealing-treated specimens as shown in Fig. 4(a). For the sealing-treated coatings, on the other hand, the mild steel substrate is protected against corrosion, but the coating corrodes more heavily than the non-sealing-treated coatings as shown in Fig. 4(b).

From the results described previously, the sealing treatment was found to protect the mild steel substrate against corrosion by closing pores, but it has a detrimental effect on the coating itself. The corrosion potentials of the coatings striped from the substrate without sealing treatment in the salt solution are −0.35 V (versus saturated calomel electrode [SCE]) for the nitrogen-atomized stainless steel coating, −0.51 V (versus SCE) for the air-atomized stainless steel coating, and −0.6 V (versus SCE) for the mild steel substrate according to the references (Ref 1, 8). Therefore, for the non-sealing-treated specimens, the substrate behaves as an anode and restrains the corrosion of the coatings. It is considered for the sealing-treated specimens that the pores were sealed so that the substrate was not available as an anode. The stainless steel coating corrodes resulting from local galvanic couplings in its inhomogeneous structure.

3.2 Corrosion Behavior in Coatings

Kelvin force microscopy is very useful in studying corrosion behavior on the microscopic scale by measuring potential distribution (Ref 6, 7). Fig. 5(a) shows the microstructure of the nitrogen-atomized coating without sealing and Fig. 5(b) and (c) show the topography and potential distribution measured by KFM in the same area as that in Fig. 5(a). The topography was caused by polishing due to the difference in hardness between the phases in the structure. The dark area shown in Fig. 5(a) is harder and its potential is higher than the light area indicated by the result of topography and potential distribution shown in Fig. 5(b) and (c), respectively. Figure 6 shows some results of EDX analysis measured at the points shown in Fig. 5(a). The dark area is considered to be an oxide and the light area is a metallic area. It is observed that the oxide phase is nobler in comparison with the metallic area and there is also a potential difference in the

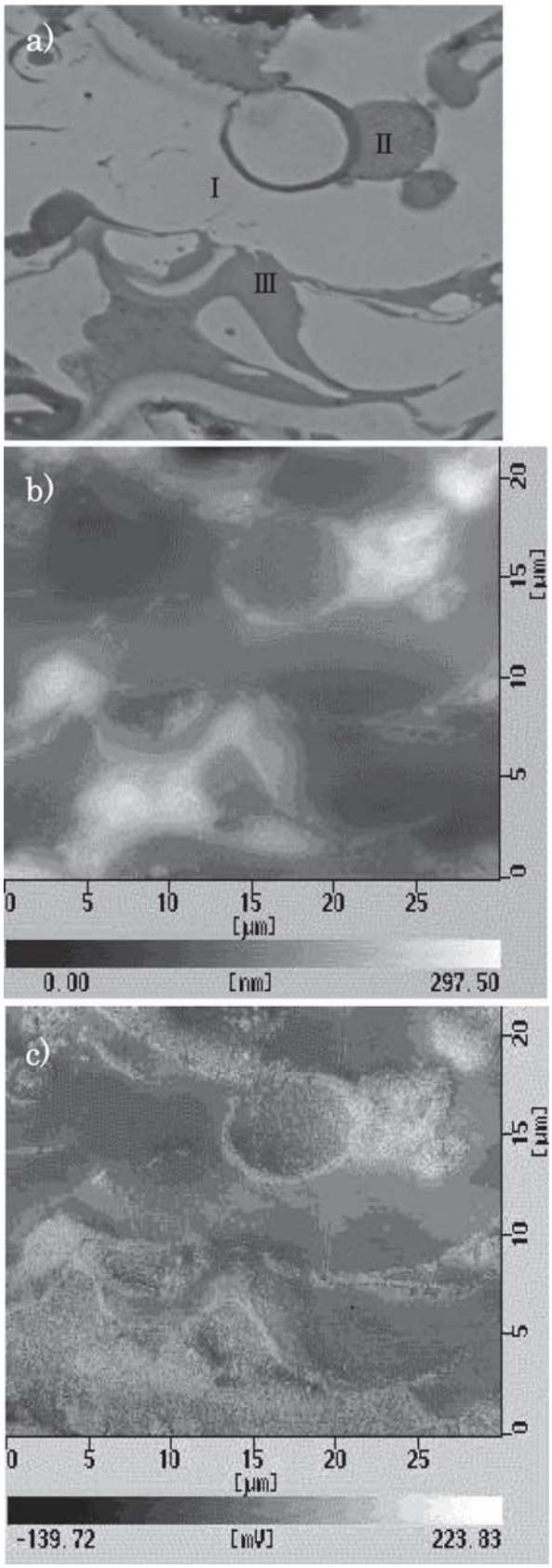

Fig. 5 SEM and KFM images of the coating on cross section; (a) SEM image, (b) topography, and (c) potential distribution

metallic area. As for the potential difference in the coating's microstructure, it is expected that galvanic cells will be formed when a coating is put in a corrosive environment, and less noble part in the metallic area would corrode as determined from the results of KFM.

To make clear the corrosion behavior of the coating itself in more detail, polished specimen was subjected to wetting/drying cycling test in 5% salt solution and the surface of the coating was observed under a microscope successively at the location. Figure 7 shows microstructures of a nitrogen-atomized coating with sealing before the test (Fig. 7a) and after the test of 250 cycles (Fig. 7b) at the specified location. The microstructures were taken from the section parallel to the surface of the coating. Three types of phase are observed in addition to the stainless steel matrix in the microstructure as shown in Fig. 7(a) (i.e., a light-gray phase labeled A, which can be distinguished from the light stainless steel matrix phase, and gray phases labeled B and C). Although B and C are not distinguished in the microstructure, the corrosion behavior is entirely different as shown in Fig. 7(b). The phases A and C corroded after the test of 250 cycles, whereas the stainless steel matrix and the gray phase B remained unaltered. This means that the phases A, B, and C differ in corrosion behavior. The gray phase B is corrosion-resistant, whereas the light-gray phase A and gray phase C are non-corrosion-resistant. The microstructures shown in Fig. 8 are taken from the cross section of the specimen before testing and after 100 and 250 cycles. The thin light gray phase A and the gray phase C corrode completely after 100 cycles. The massive light gray phase A′, however, corrodes slightly after 100 cycles and markedly after 250 cycles. The dark gray phase B does not corrode entirely after 250 cycles. The thin light-gray phase A corrodes faster than the massive light-gray phase A′. It was found from other several microstructures that the corrosion of the light gray phase depends on its size and morphology.

Figure 9 shows the microstructure and electron probe microanalyzer (EPMA) images of oxygen, iron, and chromium in the microstructure shown in Fig. 8. The light-gray phases A and A′ are both metallic and contains less chromium than the stainless steel matrix. It is shown that the gray phases, B and C are oxides, as can be seen from the microstructure and oxygen x-ray images. The oxide phase B is chromium-rich and contains iron to some extent, and the oxide, phase C is poor in chromium. The oxide phases B and C are considered as chromium-based and iron-based oxides, respectively.

The chromium-poor phase A appears always adjacent to the chromium-rich oxide phase B as shown in Fig. 7 and 8. Swank et al. (Ref 9) and Dobler et al. (Ref 10) studied oxidation in an HVOF process and described that most oxidations occur after particles impact on the substrate until next layer covers the particles. If oxidation occurs after particle's impacting, oxides may form along the surface of the particles. Because the chromium-based oxide B is present at the boundaries of particles as shown in Fig. 8(a), oxidation is expected to have occurred after droplet impingement. When a chromium-based oxide is formed after solidification, a chromium-poor region will be formed adjacent to the oxide. The adjacent locations of the chromium-based oxide and the chromium-depleted region may result from the preferential oxidation of chromium in solid state.

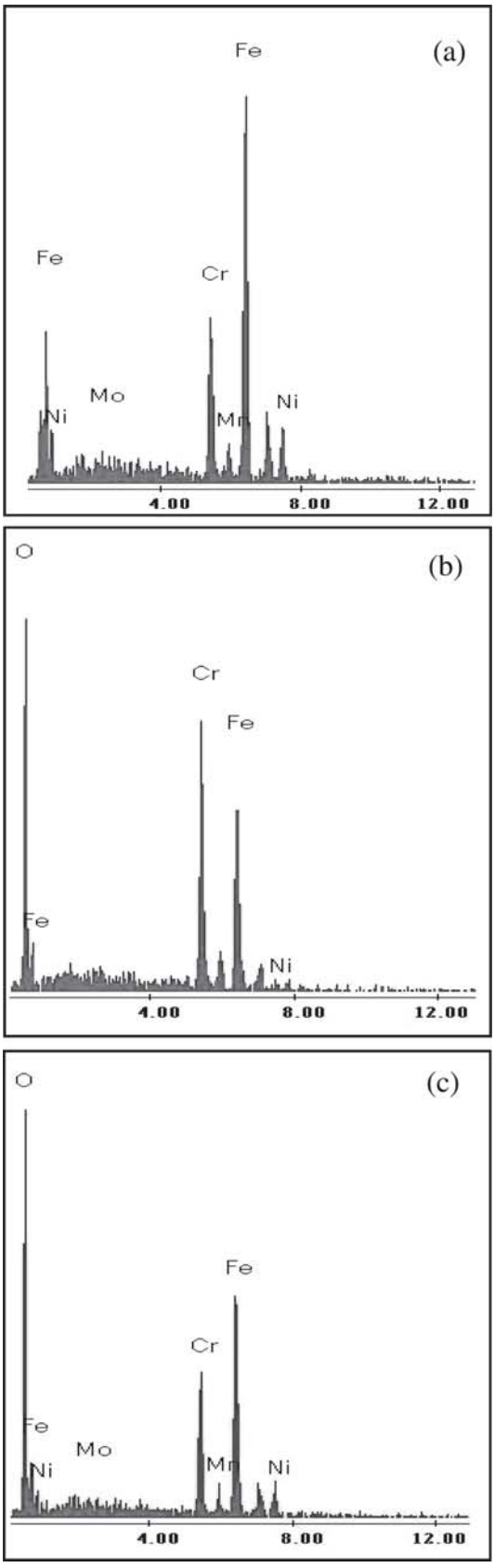

Fig. 6 Results of EDX analysis measured at the points shown in Fig. 5(a); (a) area I, (b) area II, and (c) area III

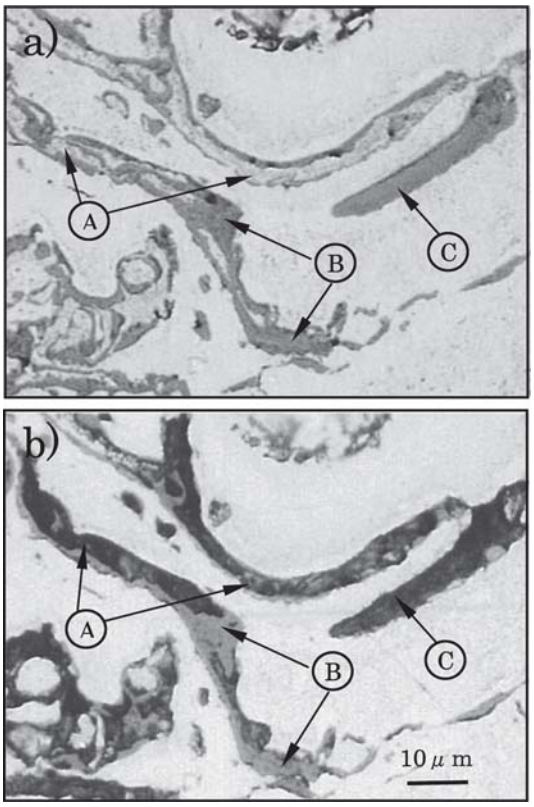

Fig. 7 Microstructures on the section parallel to the surface of the nitrogen-atomized coating; (a) before test and (b) after 250 cycles

It is clear that the iron-base oxide C corrodes easily as shown in Fig. 7 and 8, though its composition was not identified in this study. The oxide C may more likely to be formed at high temperatures in molten state as studied in wire HVOF-sprayed steel by Neiser et al. (Ref 11) The same mechanism would occur in the arc-spray process because the wire is melted almost completely in the arc, and oxidation occurs in and near the arc zone. The oxide formed in molten state could mix into the molten metal in flight and be included in the metal matrix.

It is suggested that two types of galvanic couples may exist according to the observation of the distribution of the chromium-depleted region and two species of oxides in the stainless steel matrix. One is between the chromium-based oxide as a cathode and the chromium-depleted region as an anode; the other is between the stainless steel matrix as a cathode and the iron-based oxide as an anode. The former causes the corrosion of the chromium-depleted region and the latter causes the corrosion of iron-based oxide.

4. Conclusions

The corrosion properties of wire-arc-sprayed stainless steel coatings on a mild steel substrate were investigated for specimens sprayed in different atomizing gases, and the effects of the type of atomizing gas and sealing treatment on the corrosion behavior were examined. The results are summarized as follows:

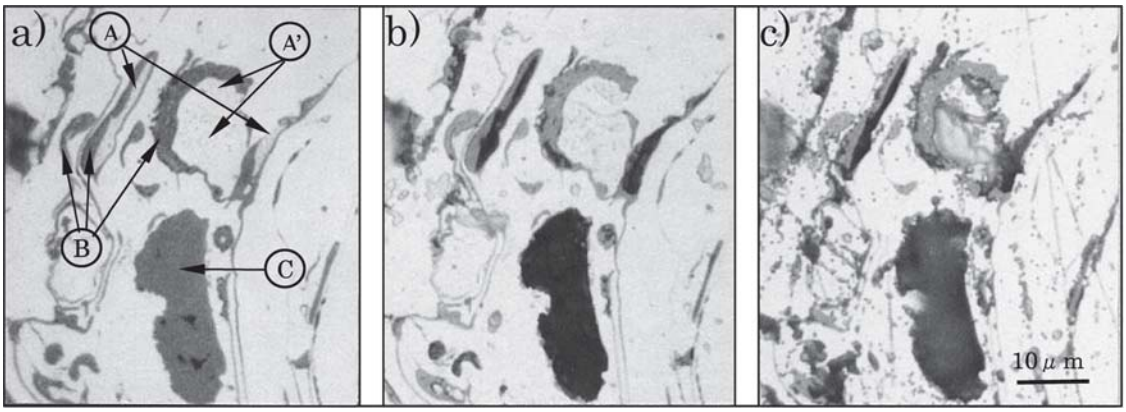

Fig. 8 Microstructures from cross section of nitrogen-atomized coating; (a) before test, (b) after 100 cycles, (c) after 250 cycles

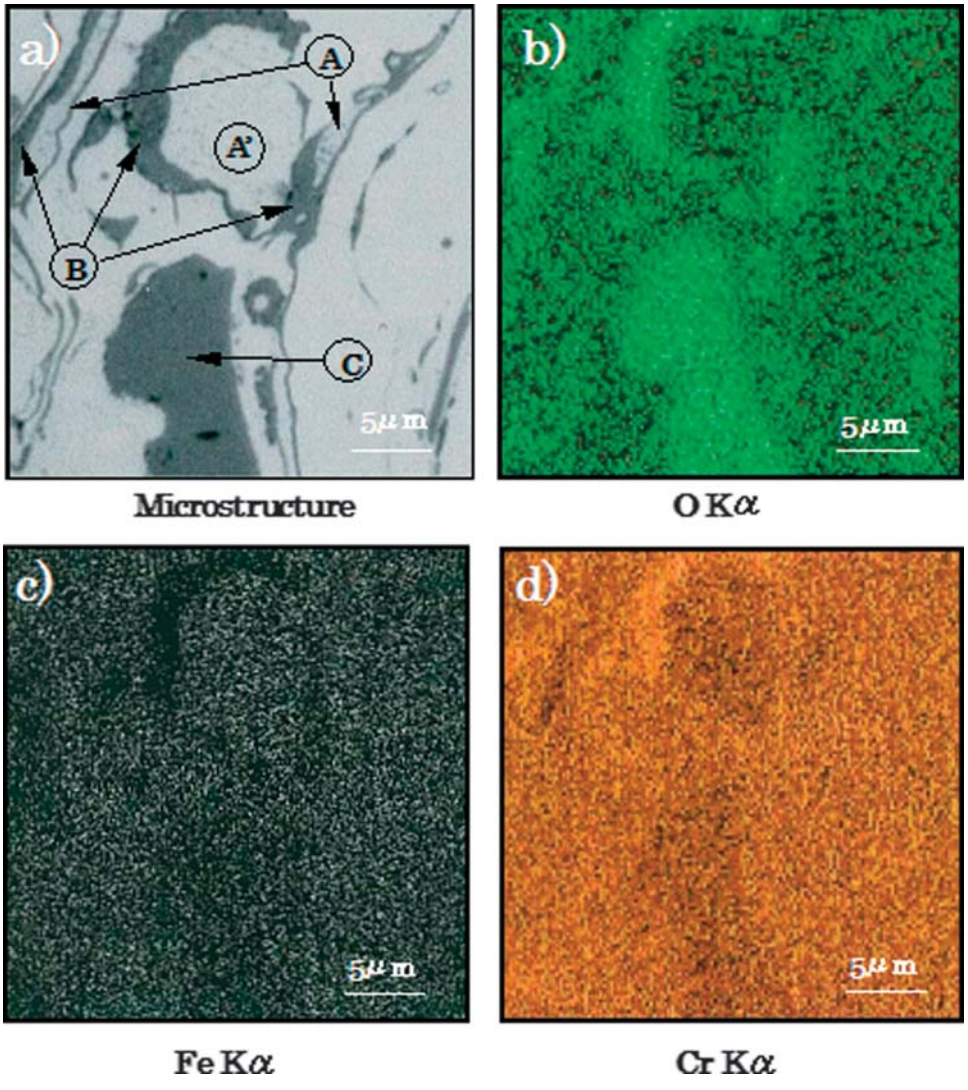

Fig. 9 (a) Microstructure by microscope and (a), (b), (c) x-ray images by EPMA analysis, at same location as the microstructure shown in Fig. 8

- Salt spray tests revealed that the sealing-treated coatings rust faster than the non-sealing-treated coatings, and that the air-atomized coatings rust more heavily than the nitrogen-atomized one for the non-sealing-treated specimens.
- The interface between the coating and the mild steel substrate corrodes greatly in the non-sealing-treated specimens and the corrosion of the coating is relatively restrained because the substrate acts as an anode.

- The substrate is protected against corrosion but the coating itself corrodes more in the sealing-treated specimens than in the non-sealing-treated specimens.
- The coating consisted of four phases in regards to corrosion behavior, that is, chromium-based oxide, iron-based oxide, chromium-depleted metallic phase, and stainless steel matrix phase. The chromium-based oxide and the stainless steel matrix phase are corrosion-resistant, whereas the chromium-depleted metallic phase and iron-based oxide are non-corrosion-resistant.

It is confirmed that sealing treatment is effective for protecting a substrate from corrosion attack. To reduce the corrosion of a sealing-treated coating, it is important to minimize the formation of the chromium-depleted metallic phase and iron-based oxide during spray process. Nitrogen atomization in wire-arc spraying forms a more reliable coating than air atomization with respect to corrosion properties.

Acknowledgments

The authors thank Prof. H. Imagawa of Torey Industries, Inc., Prof. K. Kishitake of Kyushu Institute of Technology for all discussions, and K. Tahara of Faculty of Engineering, Okayama University for KFM analysis.

References

1. M. Takemoto, Y. Longa, and G. Ueno, Metallurgical Properties and Corrosion Resistance of SUS 316L Coatings Deposited on the Carbon Steel by a Portable Atmosphere-Controlled Thermal Spraying System, *J. Corrosion Control,* 1994, **10,** p 351-357
2. T. Suzuki, K. Ishikawa, and Y. Kitamura, Corrosion Characteristics of Thermal Sprayed Stainless Steel Alloy Coating in Chloride Solution, *Thermal Spraying: Current Status and Future Trends,* Akira Ohmori, Ed., May 22-26, 1995 (Kobe, Japan), High Temperature Society of Japan, p 1033-1038, in Japanese
3. B. Arsenault, P. Gu, J.G. Legoux, B. Harvey, and J. Fournier, Stainless Steel Coating for Corrosion Protection of Steel Rebars, *Thermal Spray: Practical Solutions for Engineering Problems,* C.C. Berndt, Ed., Oct 7-11 1996, (Cincinnati, OH), ASM International, p 193-201
4. "Stainless Steel Wire for Welding," JIS G 4316, Japanese Industrial Standards Committee.
5. "Methods of Salt Spray Testing," JIS Z 2371, Japanese Industrial Standards Committee.
6. H. Masuda, Analysis of Corrosion Reaction on Metal by Kelvin Force Microscopy, *J. Surf. Sci. Japan,* 2001, **22**(5), p 282-291, in Japanese
7. H. Masuda, Analysis of Corrosion Reaction on Metal Surfaces by KFM, *J. Surf. Sci. Japan,* 1997, **18**(2), p 72-78, in Japanese
8. K. Shirai, Metallic Thermal Spray Materials, *J. High Temp. Soc.,* 1990, **16**, p 293-298, in Japanese
9. W.D. Swank, J.R. Fincke, and D.C. Haggard, HVOF Particle Flow Field Characteristics, *Thermal Spray Industrial Applications,* C.C. Berndt and S. Sampath, Eds., June 20-24, 1994 (Boston, MA), ASM International, p 319-324
10. K. Dobler, H. Kreye, and R. Schwetzke, Oxidation of Stainless Steel in the High Velocity Oxy-Fuel Process, *J. Thermal Spray Technol.,* 2000, **9**(3), p 407-413
11. R.A. Neiser, M.F. Smith, and R.C. Dykhuizen, Oxidation in Wire HVOF-Sprayed Steel, *J. Thermal Spray Technol.,* 1998, **7**(4), p 537-545